Chinese Chemical Letters 37 (2026) 112198

Contents lists available at ScienceDirect

Chinese Chemical Letters

journal homepage: www.elsevier.com/locate/cclet

pH-mediated selective self-assembly in the mitochondria of cancer cells for synergetic ferroptosis

Xuan Wu[a,*], Ming Liu[b], Xiao Wang[a], Jie Niu[c], Ting-Long Zhuang[d], Xiaohuan Sun[a], Liqi Zhu[d], Quan Zhang[d,*], Jie Han[a,*], Rong Guo[a]

[a] School of Chemistry and Chemical Engineering, Yangzhou University, Yangzhou 225002, China
[b] The Forth People Hospital of Changsha: Changsha Hospital of Hunan Normal University, Changsha 410000, China
[c] Medical College, Institute of Translational Medicine, Yangzhou University, Yangzhou 225009, China
[d] College of Veterinary Medicine, Yangzhou University, Yangzhou 225002, China

ARTICLE INFO

Article history:
Received 28 July 2025
Revised 20 November 2025
Accepted 28 November 2025
Available online 29 November 2025

Keywords:
Supramolecular self-assembly
Subcellular targeting
In situ self-assembly
Mitochondrial dysfunction
Synergetic therapy
Ferroptosis

ABSTRACT

Selective targeting to the subcellular organelle of cancer cells could provide a novel method to realize precise *in situ* self-assembly for enhanced therapeutic efficiency. Herein, a series of cationic compounds have been synthesized to investigate their subcellular targeting abilities, we found the amino group functionalized planar cationic molecules could selectively locate in the mitochondria of cancer cells (Pearson's coefficient >0.9), while in the lysosomes of normal cells (Pearson's coefficient >0.9). Moreover, due to the intermolecular hydrogen bond, the TPE derivative (TPE-NH_2) was selected to investigate the *in situ* self-assembly behavior with negatively charged molecules in the mitochondria of MB49 cancer cells, which could impair the mitochondrial membrane, leading to the elevated reactive oxygen species (ROS), down-regulating glutathione peroxidase 4 (GPX4) protein, and finally resulting in LPO for ferroptosis. Moreover, the aggregation-enhanced ROS generation ability of TPE-NH_2 made it an ideal candidate for PDT. Under the white light irradiation, the synergetic ferroptosis could be realized to suppress the cancer cell proliferation. Finally, this *in situ* self-assembly for synergetic therapy would also be realized *in vivo* to suppress the tumor growth.

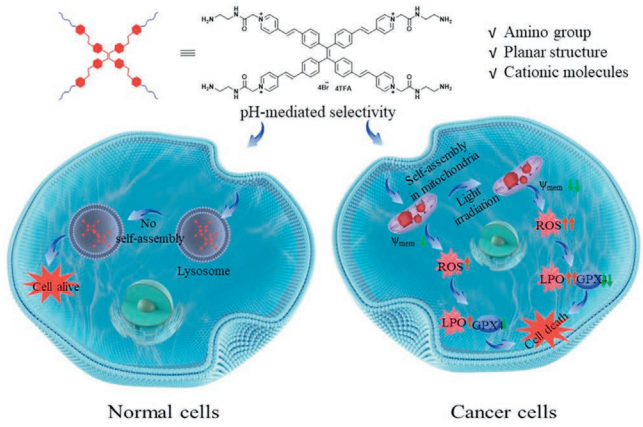
© 2026 Published by Elsevier B.V. on behalf of Chinese Chemical Society and Institute of Materia Medica, Chinese Academy of Medical Sciences.

Targeting therapy has been extensively explored due to its high drug utilization efficiency and little side effect on normal tissues [1–6]. Supramolecular self-assembly, as a convenient but efficient method to construct versatile nano-structures through non-covalent interactions, has been extensively explored in the field of therapeutic materials [7–15]. In these therapeutic systems, various targeting motifs have been incorporated for the enhanced binding with the acceptors on tumor cells, which would make the therapeutic agents efficiently accumulated in the lesion sites, while little accumulation in normal tissues. In this manner, the therapeutic agents would be efficiently taken into tumor cells and suppress their proliferation. To further realize the higher therapeutic efficiency, another targeting units would be incorporated to make the therapeutic agents directly interact with the specific organelles or bio-matters [16–20]. Even though this method could conveniently realize the targeting treatment, the introduction of multi-targeting agents would decrease the drug loading efficiency, which would intensify the metabolism burden in the further treatment. Moreover, these nano-materials exhibited relatively poor penetration ability into solid tumors, as well as disability in the transportation and storages [21–24]. Therefore, how to efficiently make the therapeutic agents work in the specific subcellular organelles of the lesion sites and not in the normal tissues seemed significant in precise treatment.

In vivo self-assembly, as a novel method to *in situ* fabricate the nano-materials in the cells or subcellular organelles, has been extensively explored in the therapeutic systems due to their intrinsic "self-assembly assisted targeting" nature [25–27]. This method could realize efficient accumulation of therapeutic agents in the lesion sites caused by the physiological environments-mediated responsiveness behavior, as well as deep penetration, which could afford an intelligent method to realize the precise targeting therapy. Traditionally, through the stimuli of physiological environments, the molecular self-assembly agents would aggregated into particular nano-structures in the lesion sites, which could remarkably improve their retention times and "turned on" their thera-

* Corresponding authors.
E-mail addresses: wuxuan@wibe.ac.cn (X. Wu), zquan@yzu.edu.cn (Q. Zhang), hanjie@yzu.edu.cn (J. Han).

https://doi.org/10.1016/j.cclet.2025.112198
1001-8417/© 2026 Published by Elsevier B.V. on behalf of Chinese Chemical Society and Institute of Materia Medica, Chinese Academy of Medical Sciences.



Scheme 1. Schematic illustration of selective assembly in the mitochondria of cancer cells for synergetic therapy.

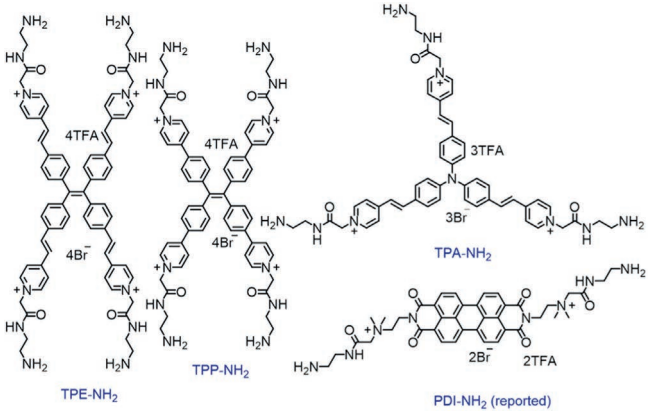


Fig. 1. Chemical structures of targeting molecules.

peutic functions [28–31]. Moreover, the introduction of subcellular targeting motifs would result in the directive interaction between nano-materials and subcellular organelles or *in situ* generation of nano-materials in subcellular organelles [32–36]. For example, Yu and co-workers fabricated a self-sorting *in situ* self-assembly system by using the peptide derivatives under the stimuli of glutathione (GSH), which could respectively interact endoplasmic reticulum and Golgi apparatus to suppress the tumor cell proliferation [37]. Xu and co-workers constructed the ALP-activated self-assembly system by using the phosphorylated peptide, which could further binding with Golgi apparatus to suppress the cell viability [38]. From the reported results, it could be concluded the different microenvironment between the normal tissues and lesion sites would result in different chemical and physical properties, as well as biofuncitons in those tissues. However, few researches were conduncted to investigate the different distribution of self-assembly agents in normal cells and affected cells. If the different distribution could be realized, these molecular agents would exhibit different self-assembly behavior in the different organelles, which would also result in different biofunction, providing a novel way for targeting treatment with high efficiency.

In the cancer tissues, the disorder metabolic processes would lead to the overexpressed bio-matters, such as high GSH [39–41], low pH [42] in the lesion sites, affording numerous method to realize targeting *in situ* self-assembly. Herein, a series of cationic compounds have been synthesized to investigated their subcellular targeting abilities, we found the amino group functionalized planar cationic molecules could selectively locate in the mitochondria of cancer cells, while in the lysosomes of normal cells (Scheme 1). To further realize this subcellular targeting ability mediated selective self-assembly in the cancer cells, a cationic tetraphenylethylene (TPE) derivative (TPE-NH_2) with intermolecular hydrogen bond was selected to investigate its *in situ* self-assembly in the mitochondira of cancer cells, driven by the multi-negatively charged molecules. Due to the stronger self-assembly behavior with multi-negatively charged molecules, the self-assembly process could lead to the enhancement in fluorescence emission as well as reactive oxygen species (ROS) generation ability. These phenomena led to the *in situ* formation of nano-materials in mitochondria of cancer cell, which resulted in the selective suppression of cancer cell proliferation. In this process, the *in situ* formed nano-particles could damage the integrity of mitochondrial membrane, elevated ROS level and downregulating the expression of glutathione peroxidase 4 (GPX4). And resulting from the assembly-enhanced ROS generation ability under the irradiation of light, the TPE-NH_2 exhibited highly efficient photodynamic therapy (PDT) for the synergetic treatment (Scheme 1). Finally, this self-assembly induced suppression of cancer cell proliferation and self-assembly-enhanced ROS generation ability could also be realized *in vivo* to suppress the tumor growth.

As is well known, the pH value of microenvironment in the normal tissues and cancer tissues is different, which has been widely applied in the pH-mediated therapeutic systems [43]. Herein, a series of amino group functionalized cationic molecules have been synthesized to explore in the colocation ability in cancer cells and normal cells. The synthesis routes were presented as Schemes S2–S4 (Supporting information). And all of these target molecules (Fig. 1) were characterized by NMR spectroscopy and HR-MS.

Then, the colocation experiment was firstly carried out on compound TPE-NH_2. As shown in Fig. 2A, the bright red fluorescence could be observed in MB49 cancer cells after incubated for 12 h, which exhibited excellent overlay with the green fluorescence arising from the commercially available Mito-tracker, indicating the TPE-NH_2 could be located in the mitochondria of MB49 cells. Moreover, the Pearson's coefficient was determined to be 0.91. Meantime, the red fluorescence assigned to TPE-NH_2 could also be observed in the normal cell (L929 cells), which exhibited ignorable colocation with commercially available Mito-tracker, whose Pearson's coefficient was 0.12 (Fig. 2B). However, a perfect overlay with lysosome-tracker could be detected, whose Pearson's coefficient was determined to be 0.96 (Fig. 2C). The same colocation experiments on L929 cells were also conducted on the model compound (TPE-Me, Scheme S1 in Supporting information), which have been reported as the mitochondrial probe of cancer cells [35]. From the obtained fluorescent images (Fig. S16 in Supporting information), the Pearson's coefficient with mitochondria was determined to be 0.43, and 0.60 with lysosomes, respectively. From the above results, it could be concluded the introduction of amino group would enable the target compound to realize specific distribution in mitochondria of cancer cells and lysosomes in normal cells.

To further certificate this principle of the ending groups mediated subcellular targeting abilities in normal cells and cancer cells. Another three compounds were further investigated. The amino group modified PDI derivative exhibited excellent colocation efficiency with mitochondria of cancer cells (MB49 cells) [35]. Then its colocation experiment in L929 cells was carried out. The same phenomena could also be observed, this compound exhibited well overlay with lysosomes of L929 cells (Fig. S17 in Supporting information), while very weak colocation within mitochondria, whose Pearson's coefficients were determined to be 0.35 and 0.96, respectively. Meantime, two more amino-functionalized compounds (TPP-NH_2 and TPA-NH_2) were also synthesized, in which the conjucated cores were changed. From the obtained fluorescence images, TPA-NH_2 could selectively located in the mitochondria of can-

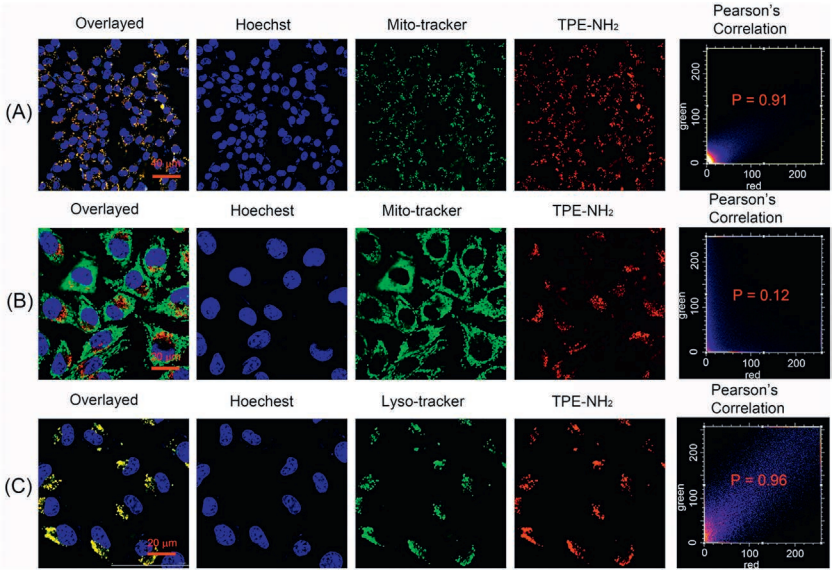


Fig. 2. Confocal laser scanning images of colocalization experiments of (A) TPE-NH_2 with the mitochondria of MB49 cells, (B) TPE-NH_2 with mitochondria of L929 cells, and (C) TPE-NH_2 with lysosomes of L929 cells ([TPE-NH_2] = 4 μmol/L).

cer cells, while in the lysosomes of normal cells (Figs. S18 and S19 in Supporting information). While the TPP-NH_2 was not located in the mitochondria of cancer cells (Fig. S19). Compared with the other molecules, the two phenyl rings in TPP-NH_2 would not be arranged co-planar due to the intrinsic steric hindrance. From the above results, it could be easily concluded the introduction of amino groups to the planar conjugated cores would enable them with the ability of specific accumulation in mitochondria of cancer cells and lysosomes in normal cells, which would have potential application in the precise treatments.

Finally, the pH-dependent properties of TPE-NH_2 were investigated by fluorescence spectroscopy. As been shown in Fig. S20B (Supporting information), the fluorescence intensity at 635 nm enhanced with the increase of pH value (from 4.0 to 8.0), which was ascribed to the aggregation-induced emission nature of TPE-NH_2. In the alkaline solution, the deprotonation of TPE-NH_2 would be occurred, accompanying with the decrease in repulsive interaction, which led to the further self-assembly of TPE-NH_2. However, the phenomena of pH-dependent fluorescence emission could not be observed in the assay of TPE-Me. From the obtained fluorescence spectra (Fig. S20A in Supporting information), no obvious change in the fluorescence intensity could be detected in the PB buffer solution (pH = 4.0–8.0).

As is well known, there has been huge amount of negatively charged molecules in mitochondria [44], such as ATP, DNA, proteins, which exhibited excellent self-assembly behavior with multi-positively charged molecules. Herein, it could be envisioned the TPE-NH_2 would realize the *in situ* self-assemble in the mitochondria of cancer cells, so its self-assembly behavior was firstly investigated by UV–vis spectroscopy using the ATP as model compound. As been shown in UV–vis titration spectra (Fig. S21B in Supporting information), the characteristic peak at 410 nm of TPE-NH_2 exhibited the hypochromatic shift to 400 nm with the gradual addition of ATP to 1.2 equiv. After that, the peak presented the bathochromic-shift to 405 nm. Moreover, the obvious scattering signal in the range of 525–600 nm would be detected in this titration process, companying with the decrease in the absorption intensity of the characteristic peak. However, little change could be observed in this titration process between TPE-Me and ATP (Fig. S21A in Supporting information). To further certificate the self-assembly behavior in presence of ATP, the transmittance

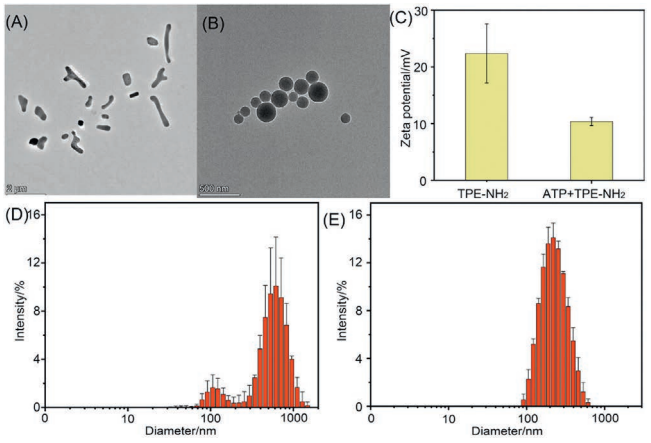


Fig. 3. (A) TEM image of TPE-NH_2. (B) TEM image of TPE-NH_2 with ATP ([TPE-NH_2]:[ATP] = 1:1.2). (C) Zeta potential values of TPE-NH_2 and the assembly of TPE-NH_2 with ATP ([TPE-NH_2]:[ATP] = 1:1.2). DLS result of TPE-NH_2 (D) and (E) TPE-NH_2 with ATP ([TPE-NH_2]:[ATP] = 1:1.2).

in the presence of ATP was also determined. From the recorded spectra (Fig. S22 in Supporting information), the transmittance of TPE-NH_2 decreased sharply upon the addition of ATP, while the transmittance of TPE-Me remained unchanged in the presence of the same amount of ATP. These phenomena indicated the introduction of amide group into the TPE derivative could enhance its self-assembly potential in the presence of multi-negatively charged molecules. Followingly, the self-assembly morphologies were also observed by using TEM. As shown in Figs. 3A and D, the irregular nanostructures of TPE-NH_2 could be observed after the evaporation of water. And the nanoparticles would be formed in the presence of ATP with the diameter around 220 nm (Figs. 3B and E), which was certificated by DLS results (Fig. 3C). Moreover, the zeta potential change in this self-assembly process also certificated this electrostatic interaction was the main driving force, concluding from the decrease in their surface potential (Fig. 2C).

Due to the aggregation-induced emission nature of TPE molecules and their derivatives, their photo-physical and photochemical properties were further investigated. From Fig. S21D (Supporting information), the characteristic emission peak of TPE-

NH_2 at 635 nm exhibited about 8-fold enhancement in the presence of 3.0 equiv. ATP. However, the emission intensity of TPE-Me showed little change in the same condition (Fig. S21C in Supporting information), which further confirmed the introduction of amide group would improve their self-assembly capability due to the synergistic effect of multi noncovalent interactions, such as electrostatic interaction, hydrogen bond, and $\pi\cdots\pi$ interaction. Furthermore, the self-assembly behavior of TPE-NH_2 in the presence of BSA and pBR322 plasmid DNA (DNA) were investigated (Fig. S23 in Supporting information), which were used as the model matters to mimic the extensively existed matters in mitochondria. From the fluorescence spectra (Fig. S23B), it could be observed the characteristic emission peak of TPE-NH_2 at 635 nm changed little with the gradual addition of BSA. And the emission intensity exhibited remarkable enhancement in the presence of DNA (Fig. S23A). Moreover, to mimic the microenvironment of mitochondria, the pH-dependent self-assembly behavior of TPE-NH_2 was investigated. As shown in Fig. S20B, the fluorescence intensity increased with the increase in the pH value, indicating this compound could self-assemble in the alkaline solution. The gradual addition of ATP into this solution (pH 8.0) would also induce the further assembly of TPE-NH_2, concluded from the fluorescence spectra (Fig. S24 in Supporting information). From the above results, it could be concluded the TPE-NH_2 exhibited excellent self-assembly properties in the presence of multi-negatively charged molecules both in the neutral and alkaline solutions, which enabled it ideal candidate for the *in situ* self-assembly in the mitochondria.

And the intramolecular donor and acceptor property of TPE-NH_2 could enhance the intermolecular charge transfer in the assembled state, enabled it an ideal candidate for ROS generation under light irradiation. Then, the photo-chemical properties of TPE-NH_2 were further investigated by using the DCFH-DA as probe. As shown in Fig. S25A (Supporting information), the probe exhibited very weak fluorescence enhancement under the white light irradiation (>400 nm, 15 mW/cm^2). The similar phenomena could also be observed in the presence of TPE-NH_2 (Fig. S25B in Supporting information), which indicated little ROS could be generated by TPE-NH_2. However, in the presence of ATP, the remarkable enhancement in fluorescence emission at 525 nm could be observed (Fig. S25C in Supporting information), indicating the much higher ROS generation ability of TPE-NH_2 in the aggregated state. Therefore, we could conclude the self-assembly of TPE-NH_2 in the presence of multi-negatively charged molecules could result in the enhancement in both the fluorescence emission and ROS generation ability of TPE-NH_2, enabling it an ideal candidate for both disease diagnosis and treatment.

Based on the above results, it could be concluded the TPE-NH_2 exhibited excellent self-assembly properties in the presence of multi-negatively charged molecules. To further investigate its physiological function, the MTT assay was carried out to investigate its effect on the cellular proliferation ability. After incubated with TPE-NH_2 for 12 h, remarkable decrease in cell viability could be observed (Fig. 4A). And the IC_{50} was calculated to be 7.16 μmol/L. Moreover, to illustrate the suppression of cellular proliferation ability was resulted from the self-assembly behavior of TPE-NH_2 in the presence of negatively charged molecules, another mitochondrial targeting compound, TPE-Me, was employed. In the same condition, little toxicity could be observed (Fig. 4B). In the same condition, the cell viability remained over 80% after the treatment of TPE-Me, indicating the excellent biocompatibility of this model compound. These phenomena might result from the intensive self-assembly behavior of TPE-NH_2 in the microenvironment of mitochondria. Due to the assembly-enhanced ROS generation ability of TPE-NH_2, its light-toxicity to cancer cells was also investigated (>400 nm, 15 mW/cm^2). As shown in Fig. 4A, more cells could be killed under the white light irradiation for 3 min, and the IC_{50} was calculated to be 2.75 μmol/L. Then its effect on normal cells was investigated. In the same condition, the proliferation ability of L929 cells was not affected without the light irradiation (Fig. S27 in Supporting information). To further illustrate this phenomenon, the flow cytometry was employed. From the obtained profiles (Fig. S28 in Supporting information), both L929 and MB49 cells exhibited similar uptake efficiency of TPE-NH_2. Therefore, the different toxicity to MB49 and L929 cells might be ascribed to the different location in the subcellular organelles of these two kinds of cells. As is well known, the proteins have been the main contents in the lysosomes, so the TPE-NH_2 in the L929 cells would not form nanostructures. However, the multi negatively charged molecules (ATP, DNA, RNA, *etc.*) in the mitochondria would drive the TPE-NH_2 to form particular nanoparticles in the MB49 cells, which might result in the excellent biocompatibility to normal cells, while high toxicity to cancer cells.

Then its anticancer mechanism was investigated. Firstly, the JC-1 probe was employed to illustrate its influence on the mitochondria. From the Confocal images (Fig. 4C), the green fluorescence in MB49 cells increased a little after treated with TPE-NH_2, whose average fluorescence intensity increased about 1.25-fold in the presence of TPE-NH_2, indicating the integrity of mitochondrial membrane was damaged (Fig. 4D). After further irradiated under white light for 3 min (>400 nm, 15 mW/cm^2), the green fluorescence exhibited the remarkable enhancement (about 1.44-fold), which indicated the mitochondrial membrane was seriously damaged under the light irradiation (Fig. 4D). These results were consistent with the previous MTT assays. To further certificated the assembly-achieved synergetic treatment in mitochondria of cancer cells, the BioTEM was carried out. From the TEM image (Fig. 5B), we could easily detect the formed nanoparticles in MB49 cells. Moreover, compared with the mitochondrial morphology in control group (Fig. 5A), the treated mitochondria shank, indicating the mitochondrial damage during this process. Another control experiment by using the pre-prepared nano-particles constructed by TPE-NH_2 and ATP was performed. Even though these nanomaterials exhibited high light-toxicity to MB49 cells (>400 nm, 3 min, 15 mW/cm^2), indicating these nano-particles could be taken into cells. However, the suppression of cellular proliferation couldn't be observed without light irradiation, indicating the pre-prepared nano-particles could not damage the mitochondrial function, which also certificated the occurrence of self-assembly in the mitochondria of MB49 cells was the main reason for suppressing cancer cell proliferation (Fig. S26 in Supporting information). From the previous literatures, the decrease in mitochondrial membrane potential could lead to the elevated ROS level in cells [45]. Then the ROS probe (DCFH-DA) was utilized to evaluate the cellular ROS level after the treatment of TPE-NH_2. After incubated with TPE-NH_2 for 12 h, the green fluorescence originated from DCFH-DA emerged (Fig. 5C), indicating the ROS level in elevated, whose average fluorescence increased about 7-fold (Fig. 5D). Moreover, the further irradiated under white light (>400 nm, 3 min, 15 mW/cm^2) would result in an enhanced green fluorescence concluded from confocal laser scanning images, and the average fluorescence increased about 1.57-fold compared with the group treated by TPE-NH_2 without light irradiation (Fig. 4D). These phenomena indicated more ROS would be generated under the light irradiation, certificating the assembly-achieved ROS generation property of TPE-NH_2.

From the above results, it could be clearly concluded the treatment of TPE-NH_2 to MB49 cells could remarkably improve the cellular ROS level, which would impair the redox-homeostasis in the cells. Then the amount of GPX4 protein was determined by western blotting experiments, which is an important protein to maintain the cellular redox-homeostasis. As shown in Fig. 6A, the GPX4 protein was downregulated by TPE-NH_2 in the dark environment, the relative GPX4 protein amount decreased to 60% (Fig.

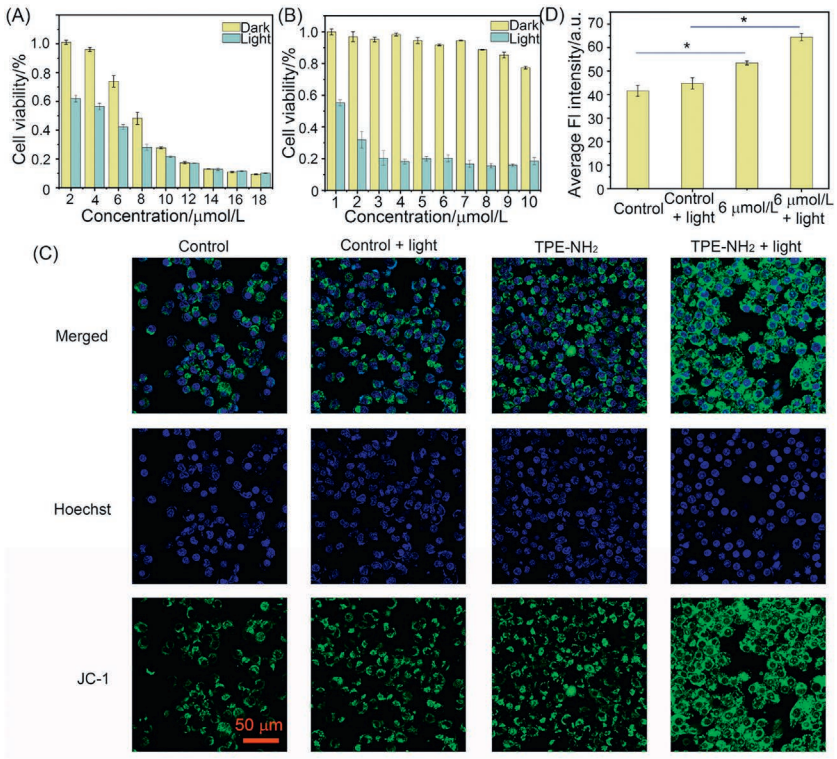


Fig. 4. (A) Concentration-dependent cell viability of MB49 cells treated with TPE-NH_2 (Data were presented as mean ± SD, $n = 5$). (B) Concentration-dependent cell viability of MB49 cells treated with TPE-Me. (C) Confocal laser scanning images of MB49 cells reflecting the mitochondrial membrane potential by using JC-1 as the probe ([TPE-NH_2] = 4 μmol/L). (D) Quantified fluorescence intensity of JC-1 images treated by TPE-NH_2 (Data were presented as mean ± SD, $n = 3$, $^{*}P < 0.05$).

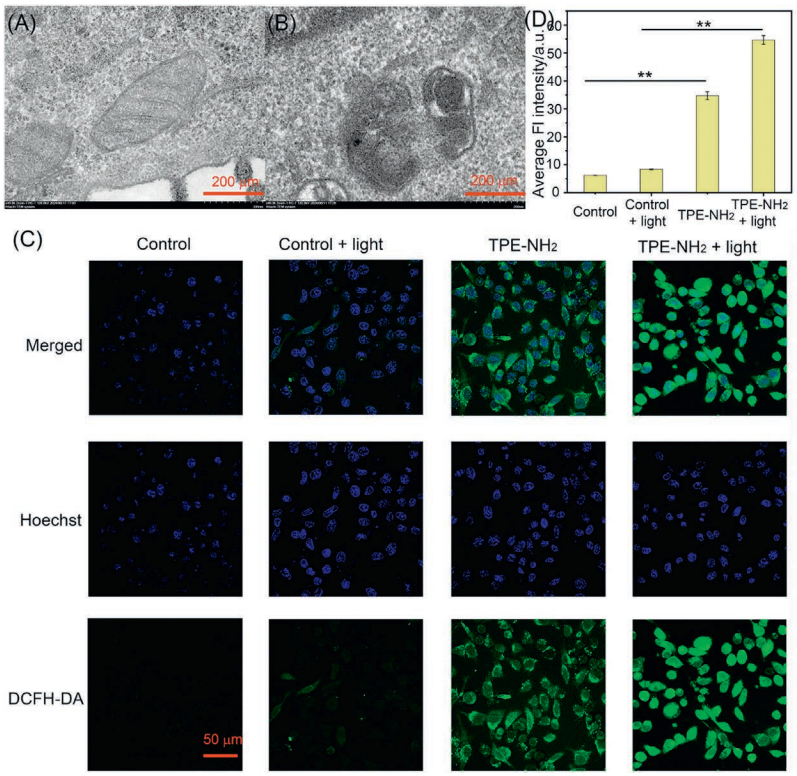


Fig. 5. BioTEM image of mitochondria treated by PBS (A) and TPE-NH_2 (B). (C) Confocal laser scanning images of MB49 cells reflecting the intracellular ROS level by using DCFH-DA probe ([TPE-NH_2] = 4 μmol/L). (D) Quantified fluorescence intensity of DCFH-DA images treated by TPE-NH_2 (Data were presented as mean ± SD, $n = 3$, $^{**}P < 0.01$).

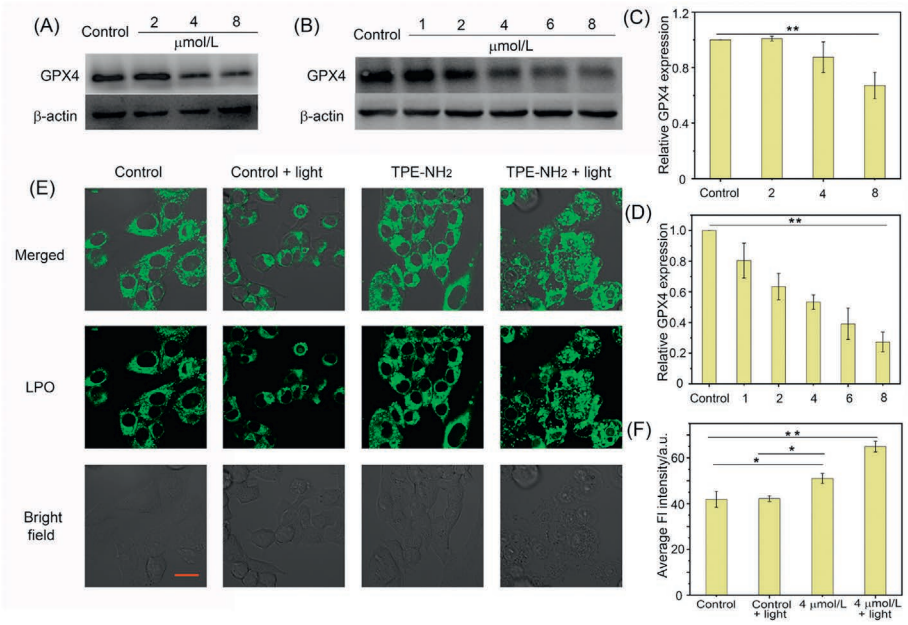


Fig. 6. (A) The membrane lipoperoxidation was evaluated by fluorescence images after staining with BODIPY^{TM}581/591 C11, where the occurrence of LPO is indicated by the enhancement in green fluorescence. (B) Quantified fluorescence intensity of LPO images treated by TPE-NH_2 (Data were presented as mean ± SD ($n = 3$), $^{*}P < 0.05$, $^{**}P < 0.01$). Western blot analysis of intracellular GPX4 expression in MB49 cancer cells treated with TPE-NH_2 (C) and TPE-NH_2 under light irradiration (D). Quantitative expression of GPX4 from Western blot analysis treated by TPE-NH_2 without (E) and with (F) light irradiation. Data were presented as mean ± SD ($n = 3$), $^{**}P < 0.01$.

6C) in the presence of 8 μmol/L TPE-NH_2, which would result in the decrease in the GSH amount in the cellular microenvironment, leading to the destruction of original redox homeostasis. Moreover, after being irradiated under white light for 3 min (>400 nm, 15 mW/cm^2), the relative GPX4 protein amount was further down-regulated, the protein amount decreased to 30% in the presence of 8 μmol/L TPE-NH_2 (Figs. 6B and D). All these results indicated the treatment of TPE-NH_2 could remarkably destroy the redox-homeostasis in MB49 cells. Finally, we further measured lipid peroxidation (LPO) of MB49 cells by using BODIPY^{TM}581/591 C11, an oxidation-sensitive LPO-specific fluorescent probe. From the obtained fluorescent images (Figs. 6E and F), the enhanced green fluorescence intensity could be detected after the treatment of TPE-NH_2 for 12 h, whose average fluorescence intensity increased by 1.2-fold, indicating that more potential for lipid peroxidation could be occurred in the presence of TPE-NH_2. And the continual irradiation under white light (>400 nm, 15 mW/cm^2) would further enhance the green fluorescence, indicating the damage of the redox homeostasis resulted from the synergetic treatment of TPE-NH_2. Moreover, this TPE-NH_2-mediated LPO processes also exhibited the concentration-dependent phenomena. From the obtained Confocal laser scanning images (Figs. S29–S32 in Supporting information), the green fluoscence increased with the TPE-NH_2 concentration. From the above results, it could be concluded that TPE-NH_2 could be concentrated in the mitochondria of MB49 cancer cells, which could lead to the decrease in mitochondrial membrane potential, and the increase of ROS level in the cytoplasm. These phenomena could further destroy the cellular redox homeostasis and down-regulate the GPX4 protein, leading to lipid peroxidation. Therefore, a ferroptosis-like system was successfully constructed through the self-assembly of TPE derivative in the mitochondria of cancer cells.

Finally, the *in vivo* experiments were also conducted to further investigate its anti-tumor efficiency (Fig. 7A), in which the MB49 tumor model on the mice was established (approved by the Science and Technology Department of Jiangsu Province and conducted with the approval of the Medical Ethics Committee of Yangzhou University Medical Academy (YXYLL-2022–44)). As shown in Figs. 7B and C, after being treated for 12 days, both the tumor volume and weight were much smaller than those in the group treated by PBS. And the final tumor weight of TPE-NH_2 in the dark environment was (0.47 ± 0.1) g, indicating the tumor growth was successfully suppressed after treated by TPE-NH_2, while little effect on the growth of mice, whose body weight was not affected after the treatment (Fig. 7E). Moreover, the tumors almost dismissed in the irradiation group after 3 day's treatment (405 nm, 5 min, 50 mW/cm^2), and would not relapsed without the further administration of TPE-NH_2 (Fig. S33 in Supporting information). Finally, we also conducted immunohistochemical staining by collecting the tumors after 2 day's treatment. From the H&E staining of tumor slices (Fig. 7F), an obvious decrease in the number of nuclei could be observed after administration of TPE-NH_2, compared with the compact nuclei in the groups treated with PBS. This phenomenon indicated the tumor tissues suffered destruction after the treatment. The Ki67 staining was also performed to investigate the proliferation ability of tumor cells. From Fig. 7G, fewer Ki67^{+} cells could be observed after the treatment of TPE-NH_2, indicating the proliferation ability of tumor cells decreased sharply after the treatment. Therefore, it could be concluded the TPE-NH_2 could suppress the tumor growth. The safety of TPE-NH_2 was further investigated on BALB/c mice. After injected with the solution containing TPE-NH_2 through the tail vein for 12 days, the main organs (heart, liver, spleen, lung, and kidney) were also collected. Then the H&E staining was performed (Fig. S34 in Supporting information). Compared with PBS-treated mice, H&E staining also indicated that TPE-NH_2 possessed ignorable long-term toxicity to the main organs, and these results indicated the excellent biocompatibility of these *in situ* self-assembly system.

Herein, a kind of amino group functionalized cationic molecules has been successfully synthesized, which could selectively locate in the mitochondria of cancer cells, while in the lysosomes of normal cells. Due to the multi-noncovalent interaction between these molecules (hydrogen bonding, $\pi\cdots\pi$ stacking), they exhibited excellent assembly behavior in the presence of multi-negatively charged molecules. Therefore, we synthesized a TPE derivative

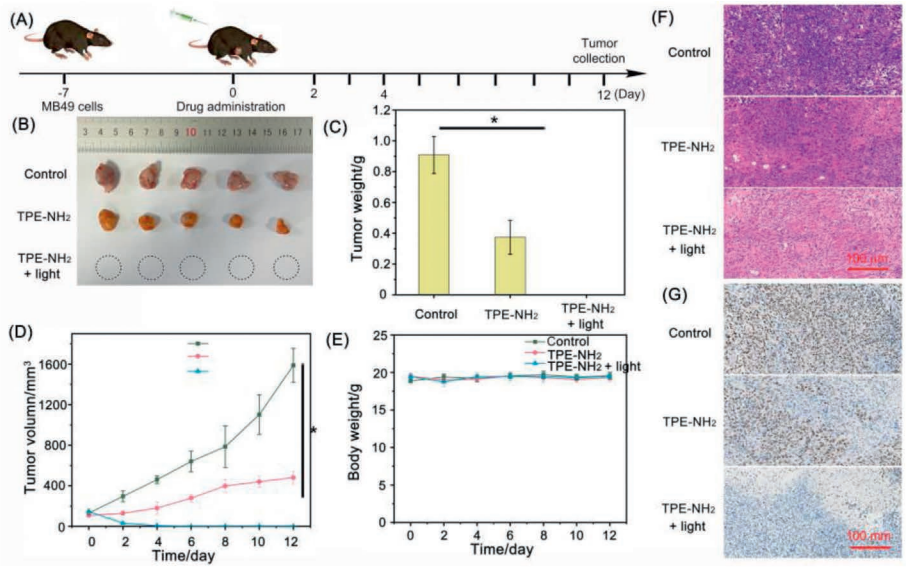


Fig. 7. (A) The schematic diagram of tumor inoculation and therapy. (B) Photo of the MB49 tumors collected on day 12 (Data were presented as mean ± SD, $n = 5$). (C) Weight of MB49 tumors at day 12 (Data were presented as mean ± SD, $n = 5$, $^{*}P < 0.05$). (D) Tumor growth curves of MB49 on the BALB/c mice (Data were presented as mean ± SD, $n = 5$, $^{**}P < 0.01$). (E) Body weight curves of MB59-bearing mice ($n = 5$). (F) H&E, and (G) Ki67 staining of tumors after the treatment for 12 days.

(TPE-NH_2), which could selectively concentrate in the mitochondria of MB49 cells, and then self-assemble into nanoparticles through the electrostatic interaction with the ATP or DNA in mitochondria. The results indicated the formed nanoparticles could impair the mitochondrial membrane, leading the elevated ROS, as well as downregulating GPX4 protein for the further LPO, which could suppress the cancer cell viability, while exhibited little toxicity to normal cells. Moreover, due to the aggregation-enhanced ROS generation ability of TPE-NH_2, the formed nanoparticles also exhibited very intensive light-toxicity under the white light irradiation, which could also impair the mitochondrial membrane, downregulate GPX4 protein, as well as lead to LPO for suppressing cancer cell proliferation. Finally, this *in situ* self-assembly system in mitochondria of cancer cells could also be realized *in vivo* to suppress the tumor growth, while exhibited excellent biocompatibility. This self-assembly mediated targeting therapeutic method could avoid side effect to normal tissues, in which the nanomedicine could be specifically fabricated under the stimulation of the physiological environment in lesion sites. Moreover, this pH-mediated selective self-assembly in cancer cell mitochondria for synergistic therapy without other targeting motifs might provide a novel way to realize the highly efficient therapy.

CRediT authorship contribution statement

Xuan Wu: Writing – review & editing, Writing – original draft, Validation, Supervision, Methodology, Investigation, Funding acquisition, Data curation, Conceptualization. **Ming Liu:** Writing – original draft, Validation, Investigation. **Xiao Wang:** Writing – original draft, Investigation, Data curation. **Jie Niu:** Writing – original draft, Investigation, Data curation. **Ting-Long Zhuang:** Investigation, Data curation. **Xiaohuan Sun:** Writing – review & editing, Supervision. **Liqi Zhu:** Supervision, Conceptualization. **Quan Zhang:** Writing – review & editing, Supervision, Conceptualization. **Jie Han:** Writing – review & editing, Supervision, Project administration, Funding acquisition, Conceptualization. **Rong Guo:** Supervision, Project administration.

Declaration of competing interest

The authors declare that they have no known competing financial interests or personal relationships that could have appeared to influence the work reported in this paper.

Acknowledgments

This work was supported by the National Natural Science Foundation of China (Nos. 22101280, 22272146) and the Priority Academic Program Development of Jiangsu Higher Education Institutions.

Supplementary materials

Supplementary material associated with this article can be found, in the online version, at doi:10.1016/j.cclet.2025.112198.

References

[1] B.A. Carneiro, W.S. El-Deiry, Nat. Rev. Clin. Oncol. 17 (2020) 395–417.
[2] W. Huang, F. Yao, S. Tian, et al., Pharmaceutics 15 (2023) 1820.
[3] S. Lei, J. He, P. Gao, et al., Mol. Imaging Biol. 25 (2023) 1020–1033.
[4] J. Liu, J. Shi, W. Nie, et al., Adv. Healthcare Mater. 10 (2021) 2001207.
[5] Y. Qu, W. Jin, Y. Wan, et al., Chin. Chem. Lett. 35 (2024) 108493.
[6] C. Lin, C. Huang, Z. Shi, et al., Acta Pharm. Sin. B 12 (2022) 4472–4485.
[7] Y. Chen, S. Sun, D. Lu, et al., Chin. Chem. Lett. 30 (2019) 37–43.
[8] X. Li, M. Shen, J. Yang, et al., Adv. Mater. 36 (2024) 2313317.
[9] Y.Y. Liu, X.Y. Yu, Y.C. Pan, et al., Sci. China Chem. 67 (2024) 1397–1441.
[10] Z. Liu, Y. Liu, Chem. Soc. Rev. 51 (2022) 4786–4827.
[11] M.J. Webber, R. Langer, Chem. Soc. Rev. 46 (2017) 6600–6620.
[12] X. Wu, L. Gao, X.Y. Hu, et al., Chem. Rec. 16 (2016) 1216–1227.
[13] Q. Ren, X. Dai, R. Cen, et al., Chin. Chem. Lett. 35 (2024) 110022.
[14] Y. Zhang, X. Yu, L. Luo, et al., J. Control. Release 376 (2024) 1115–1129.
[15] H. Zhang, Y. Zhang, Y. Zhang, et al., Nat. Commun. 15 (2024) 6783.
[16] J.I. Joo, M. Choi, S.H. Jang, et al., Adv. Mater. 32 (2020) 1906783.
[17] S. Louzoun-Zada, Q.Z. Jaber, M. Fridman, Angew. Chem. Int. Ed. 58 (2019) 15584–15594.
[18] S. Wang, P. Huang, X. Chen, Adv. Mater. 28 (2016) 7340–7364.
[19] Y. Wu, W. Chen, C. Wang, et al., Chin. Chem. Lett. 35 (2024) 109096.
[20] Y. Zheng, Y. Oz, Y. Gu, et al., Nano Today 55 (2024) 102147.
[21] Y. Cheng, Z. Qu, Q. Jiang, et al., Adv. Mater. 35 (2023) 2305095.
[22] Z. Fang, H. Chen, Adv. Drug. Deliv. Rev. 200 (2023) 115020.
[23] Y. Sato, T. Nakamura, Y. Yamada, et al., J. Control. Release 370 (2024) 516–527.
[24] H. Su, G. Rong, L. Li, et al., Adv. Drug. Deliv. Rev. 212 (2024) 115387.
[25] J. Ding, J. Chen, L. Gao, et al., Nano Today 29 (2019) 100800.
[26] M.O. Durymanov, A.A. Rosenkranz, A.S. Sobolev, Theranostics 5 (2015) 1007–1020.

[27] M. Mamuti, R. Zheng, H.W. An, et al., Nano Today 36 (2021) 101036.
[28] W. Du, X. Hu, W. Wei, et al., Bioconjugate Chem. 29 (2018) 826–837.
[29] L.L. Li, Z.Y. Qiao, L. Wang, et al., Adv. Mater. 31 (2019) 1804971.
[30] X. Mo, Z. Zhang, J. Song, et al., J. Mater. Chem. B 12 (2024) 4289–4306.
[31] S.Y. Qin, J.Q. Feng, Y.J. Cheng, et al., Coord. Chem. Rev. 502 (2024) 215600.
[32] S. Kim, H. Choi, S. Jin, et al., Giant 16 (2023) 100189.
[33] J. Niu, J. Yu, X. Wu, et al., Chem. Sci. 15 (2024) 13779–13787.
[34] X. Wu, M. Liu, J. Niu, et al., Chem. Sci. 14 (2023) 1724–1731.
[35] X. Wu, T.L. Zhuang, M. Liu, et al., Org. Chem. Front. 11 (2024) 6055–6063.
[36] Q. Zhang, W. Tan, B. Xu, ChemPlusChem 87 (2022) e202200060.
[37] X. Liu, F. Tian, Z. Zhang, et al., J. Am. Chem. Soc. 146 (2024) 24177–24187.
[38] W. Tan, Q. Zhang, J. Wang, et al., Angew. Chem. Int. Ed. 60 (2021) 12796–12801.
[39] N. Kang, S. Son, S. Min, et al., Chem. Soc. Rev. 52 (2023) 3955–3972.
[40] S. Sheng, Y. Zhang, L. Jin, et al., Nat. Commun. 16 (2025) 6045.
[41] Y. Yi, Z. Peng, Y. Liu, et al., Acta Pharm. Sin. B 15 (2025) 2237–2252.
[42] P. Swietach, E. Boedtkjer, S.F. Pedersen, Nat. Rev. Cancer 23 (2023) 825–841.
[43] Y. Song, H. Zhang, X. Wang, et al., Anal. Chem. 93 (2021) 1786–1791.
[44] P.E. Porporato, N. Filigheddu, J.M.B.S. Pedro, et al., Cell Res. 28 (2018) 265–280.
[45] Z. Liu, X. Wang, Q. Chen, et al., Angew. Chem. Int. Ed. 60 (2021) 16215–16223.